A Journal of the Gesellschaft Deutscher Chemiker

Angewandte International Edition GDCh Chemie

www.angewandte.org

Accepted Article

Title: Electrochemical Capacitance Traces with Interlayer Spacing in Two-dimensional Conductive Metal-Organic Frameworks

Authors: Alice Su, Petru Apostol, Jiande Wang, Alexandru Vlad, and Mircea Dincă

To be cited as: *Angew. Chem. Int. Ed.* **2024**, e202402526

Link to VoR: https://doi.org/10.1002/anie.202402526

WILEY VCH

10.1002/anie.202402526

WILEY VCH

COMMUNICATION

Electrochemical Capacitance Traces with Interlayer Spacing in Two-dimensional Conductive Metal-Organic Frameworks

Alice Y. Su[a], Petru Apostol[b], Jiande Wang[a], Alexandru Vlad[b] and Mircea Dincă*[a]

[a] A. Su, Dr. J. Wang, Prof. Dr. M. Dincă
Department of Chemistry
Massachusetts Institute of Technology
Cambridge (USA)
E-mail: mdinca@mit.edu

[b] Dr. P. Apostol, Prof. Dr. A. Vlad
Institute of Condensed Matter and Nanosciences, Molecular Chemistry, Materials and Catalysis
Université Catholique de Louvain
Louvain-la-Neuve B-1348, Belgium

Supporting information for this article is given via a link at the end of the document.

Abstract: Electrically conductive metal-organic frameworks (MOFs) are promising candidates for electrochemical capacitors (EC) for fast energy storage due to their high specific surface areas and potential for redox activity. To maximize energy density, traditional inorganic pseudocapacitors have utilized faradaic processes in addition to double-layer capacitance. Although conductive MOFs are usually comprised of redox active ligands which allow faradaic reactions upon electrochemical polarization, systematic studies providing deeper understanding of the charge storage processes and structure-function relationships have been scarce. Here, we investigate the charge storage mechanisms of a series of triazatruxene-based 2D layered conductive MOFs with variable alkyl functional groups, $Ni_3(HIR_3\text{-}TAT)_2$ (TAT = triazatruxene; R = H, Et, *n*-Bu, *n*-Pent). Functionalization of the triazatruxene core allows for systematic variation of structural parameters while maintaining in-plane conjugation between ligands and metals. Specifically, R groups modulate interlayer spacing, which in turn shifts the charge storage mechanism from double-layer capacitance towards pseudocapacitance, leading to an increase in molar specific capacitance from $Ni_3(HIH_3\text{-}TAT)_2$ to $Ni_3(HIBu_3\text{-}TAT)_2$. Partial exfoliation of $Ni_3(HIBu_3\text{-}TAT)_2$ renders redox active ligand moieties more accessible, and thus increases the dominance of faradaic processes. Our strategy of controlling charge storage mechanism through tuning the accessibility of redox-active sites may motivate further design and engineering of electrode materials for EC.

Electrochemical capacitors (EC) bridge the gap between traditional parallel plate capacitors and batteries in terms of energy and power density.[1] Pure double-layer capacitors store energy via the formation of electrochemical double layers (EDL) consisting of physisorbed electrolyte ions. In ideal EDL capacitors, the specific surface area of the active electrode material is directly proportional to the amount of charge stored.[2] However, this charge storage capacitance can be supplemented by rapid Faradaic processes in materials such as $RuO_2{\cdot}xH_2O$ and Nb_2O_5, which are said to operate as pseudocapacitors.[3] Non-porous coordination polymers have also been demonstrated to deliver high capacitance due to faradaic cation intercalation.[4,5] Electrically conductive 2D metal-organic frameworks (c-MOFs) are porous hybrid organic-inorganic materials that have emerged as viable materials for supercapacitors based on their high specific surface areas and efficient charge transport.[6–8] In many conductive MOFs, redox active ligands engage in charge transfer processes, leading to improved energy densities, while porosity increases ion access to the redox sites.[9,10] Importantly, the role of confinement of electrolyte ions in the pores of layered materials has received a lot of attention, revealing that matching of ion and pore size can lead to ion desolvation and greater charge density.[11–13] Yet, exploring specific aspects of charge storage in EC has been difficult because changing composition leads to multiple structural and/or physical changes that are challenging to deconvolute.

Due to their high tunability, c-MOFs serve as an excellent platform to rationally vary structural properties to probe charge storage with a wholistic view of both electronic and mass transport mechanisms. Recently, ligand tuning by alkylation of the triazatruxene (TAT) ligands before assembly to 2D TAT MOFs has been demonstrated.[14–16] It has been shown that the specific surface area of this family of MOFs can be tuned by changing the length of alkyl chains occupying the free pore space. Additionally, the stacking distance of the 2D sheets is likewise dependent on the alkyl substituents disturbing the interlayer π-stacking interactions. This enables the investigation of the effects of interlayer spacing and pore size on the capacitive mechanisms. Herein, we show that with c-MOFs, there is a direct relationship between interlayer spacing and capacitance and that, surprisingly, increasing the interlayer spacing causes a shift in the mechanism of charge storage itself, from physical capacitance to a large contribution of faradaic pseudocapacitive processes.

Solvothermal reaction between nickel acetate and variously *N*-functionalized hexaaminotriazatruxene (HATAT) ligands in aqueous sodium acetate/ *N*,*N*-dimethylformamide/ *N*,*N*-dimethylacetamide yields four isostructural HATAT-based hexagonal 2D layered c-MOFs with the general formula $Ni_3(HIR_3\text{-}TAT)_2$ (R = -H, -Et, -*n*-Bu, -*n*-Pent; abbreviated as H-MOF, Et-MOF, Bu-MOF, and Pent-MOF, respectively) (**Figures 1a, b and S1**).[15,16] We found that with these TAT-based MOFs, longer alkyl chains lead to more rapid precipitation, yielding materials with lower crystallinity under otherwise identical synthetic conditions. Increasing the pH of the reaction mixture through the addition of increasing amounts of sodium acetate improves the crystallinity of Pent-MOF (**Figure S2**). Infrared spectra of the frameworks

10.1002/anie.202402526

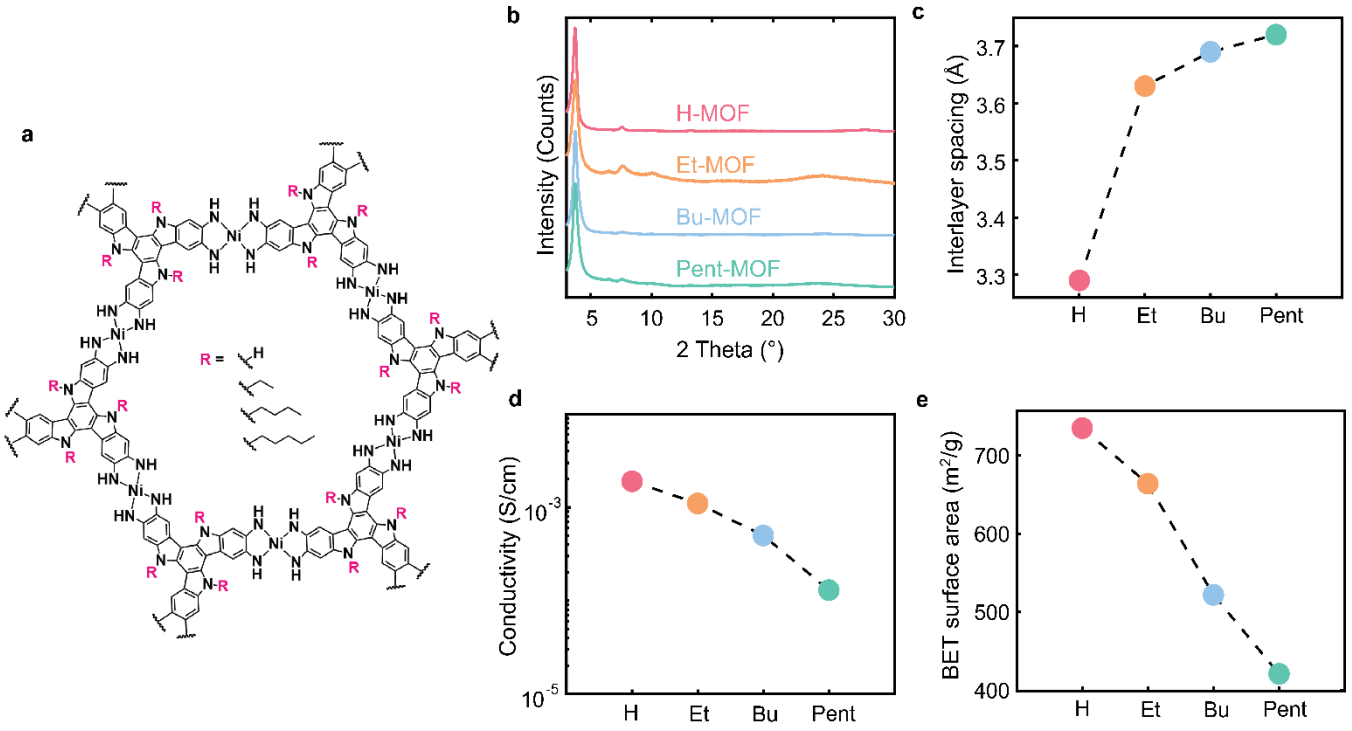

Figure 1. a) Molecular structure of $Ni_3(HIR_3\text{-}TAT)_2$ in the ab-plane. R = H, Et, n-Bu, n-Pent. b) PXRD patterns of H-MOF, Et-MOF, Bu-MOF and Pent-MOF. c) Progression of interlayer spacings across the series of MOFs, determined from [001] reflections d) Electronic conductivities and e) BET surface areas of MOFs

show increasing relative intensities of alkyl C–H stretching bands when going from H-MOF to Et-MOF, Bu-MOF, and Pent-MOF (**Figure S3**). Powder X-ray diffraction analysis demonstrated that all four MOFs display comparable in-plane structural order, as verified by the similar full-widths-at-half-maximum values, ~0.5°, of the [100] reflections at 2θ = 3.76° (**Figure S4 and Table S1**). The stacking distance of the 2D sheets increases with increasing alkyl chain length from 3.29 Å for H-MOF to 3.63 Å, 3.69 Å and 3.72 Å for Et-MOF, Bu-MOF and Pent-MOF, respectively, as calculated from the [001] reflections between 2θ = 23° and 28° (**Figure 1c**). The attenuated π-π stacking interaction induced by increasing the alkyl chain length leads to lower electronic coupling in the *c*-direction and reduced band dispersion, ultimately decreasing electrical conductivity from 1.9 mS/cm for H-MOF to 1.1 mS/cm, 0.50 mS/cm, and 0.13 mS/cm for Et-MOF, Bu-MOF and Pent-MOF, respectively (**Figure 1d**). N_2 sorption isotherms at 77 K gave apparent BET surface areas that decrease with chain length due to the alkyl chains residing in the pores: 735 m^2/g, 664 m^2/g, 522 m^2/g, and 421 m^2/g for H-MOF through Pent-MOF (**Figures 1e, S5** and **Table S2**). The total pore volume similarly decreases with increasing alkyl chain length.

The foregoing analytical data confirm that side chain engineering of the organic linker modulates the interlayer distance, specific surface area, and accessible pore volumes of this series of TAT-based 2D conductive MOFs. As such, this family of frameworks serves as an ideal platform to correlate structurally induced effects with charge storage behaviour; electronic effects, dominated by in-plane conjugation and minimally influenced only

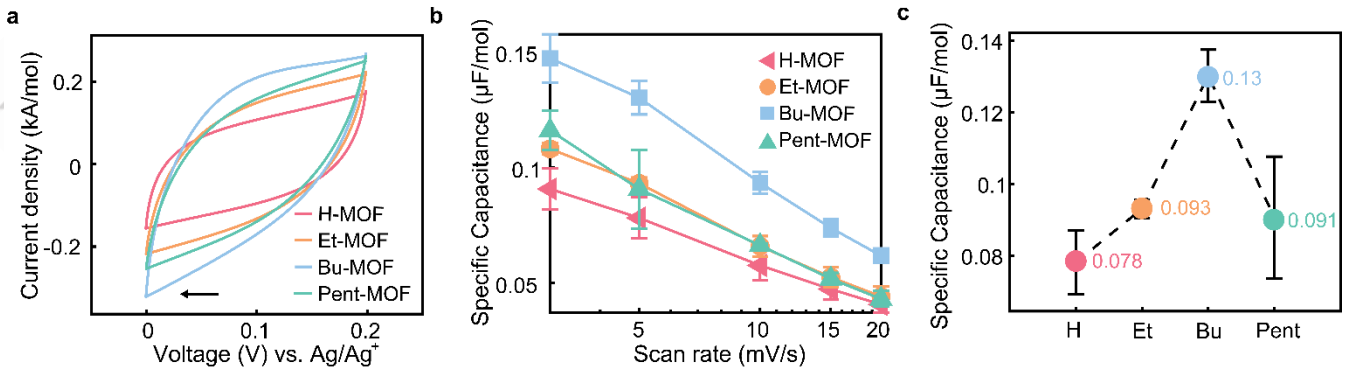

Figure 2. a) CV traces of c-MOFs in three electrode cells from 0.2 V to 0.0 V vs. Ag-wire pseudo-reference. The second cycle is shown. Molar current densities are normalized vs. moles of TAT ligand. b) Molar specific capacitances (normalized vs. moles of TAT ligand) determined from CV scans at scan rates from 3 to 20 mV/s. c) Comparison of molar specific capacitances at a scan rate of 5 mV/s.

10.1002/anie.202402526

by the degree of interlayer band dispersion, are effectively decoupled from structural changes.[13]

Electrochemical characterization was performed in a three-electrode configuration. A mixture of c-MOF and conductive carbon with a mass ratio of 9:1 was pressed directly onto nickel foam as the working electrode, whereas an activated carbon pellet electrode with at least ten times higher mass than the MOF was used as the counter electrode. A LiTFSI (TFSI = trifluoromethanesulfonylimide) 1 M solution in acetonitrile was identified as a suitable electrolyte due to the large accessible voltage window of acetonitrile and stability of the c-MOFs in this solvent (**Figure S6**). Cyclic voltammetry (CV) shows quasi-rectangular traces for all four materials in cathodic sweeps from 0.2 V to 0.0 V referenced against a silver wire pseudo-reference electrode (**Figures 2a and S7**). The molar specific capacitances (given per mol of TAT ligand) were determined from CV scans at scan rates between 3 mV/s and 100 mV/s. At low scan rates up to 20 mV/s, the molar specific capacitance increases with increasing interlayer distance from H-MOF to Et-MOF to Bu-MOF by up to a factor of 1.7 but decreases from Bu-MOF to Pent-MOF (**Figure 2b,c and Figure S8**). Because specific capacitance and specific surface area follow inverse trends across the series of c-MOFs, it can be inferred that a second capacitive component, likely faradaic, contributes to the overall capacitance and it increases with alkyl chain length and interlayer distance.

The decrease in specific capacitance from Pent-MOF to Bu-MOF can experimentally be assigned to a continuously increasing ion transport resistance with increasing alkyl chain length; when R = *n*-Pent, ion transport cannot compensate the rapidly charging capacitor of Pent-MOF. A first sign of this is the width of the CV trace for Pent-MOF, which shows the narrowest cycle, more typical for resistors (**Figure 2a**). Analysis of the scan rate dependence of the CV currents using the power law $i = av^b$ provides insight into diffusion resistances. The current i is hereby expressed as a constant factor, a, multiplied by the scan rate v to the power of a factor b, which can assume values between 0.5 and 1. In the lower limit of b = 0.5, the current is proportional to the square root of the scan rate, which indicates an ideal semi-infinite diffusion regime, as described by the Randles-Ševčík equation.[17] For surface-adsorbed species, where no mass transfer limitations are at play, b = 1.[17] Here, the b-values fitted for scan rates from 3 to 20 mV/s show a decreasing trend from 0.69 for H-MOF to 0.51 for Pent-MOF, pointing to increasing mass transfer limitations as the alkyl group becomes longer (**Figures 3a, S9 and Table S3**). Electrochemical impedance spectroscopy (EIS) performed at frequencies between 10 mHz and 500 kHz provided additional insight in the dynamic behaviour of the electrode materials under various degrees of electrochemical polarization. Nyquist plots of the four materials reveal low equivalent series resistances of 1-2 Ω and overlapping semicircles at high frequencies, leading to a diffusion dominated regime, and capacitive tail that deviates from the vertical, typical for non-ideal porous supercapacitors (**Figure S10**). The diameters of the semicircles can be understood as the combination of interfacial and charge-transfer resistances. The onset of the quasi-linear tails moves to higher resistances with increasing chain length.[18]

CV analysis reveals increasingly faradaic behaviour from H-MOF to Pent-MOF. By extending the voltage window of the cathodic sweep to −0.4 V, a broad faradaic feature emerges for the alkylated frameworks around −0.1 V, whereas H-MOF shows a smooth current response without signs of localized charge transfer induced current peaks (**Figure 3b**). Although scans from 0.2 to 0.0 V do not exhibit distinct faradaic peaks for any materials, the broad onset of the charge transfer peak at −0.1 V is likely to contribute to the capacitance in the smaller voltage window.

Similar to DC techniques, AC analysis shows a clear trend of increasing resistance from H-MOF to Pent-MOF. This progression is, however, overshadowed by faradaic processes that become more prominent with interlayer spacing, dominating the charge transfer mechanism for the most part. EIS at different electrochemical polarizations shows contributions of voltage dependent charge transfer resistances. Although the semicircle diameters in the Nyquist plot remain at almost the same real impedance for H-MOF, an increasingly stronger voltage dependence is observed for the alkylated MOFs (**Figure 3c, d**). Bode-style projections (**Figure 4**) show that the voltage dependence of the real capacitance at low frequencies increases with increasing interlayer spacing, as seen in the more pronounced dome-shapes. This indicates an increasing contribution of charge transfer (i.e. faradaic) processes to the real capacitance.[19]

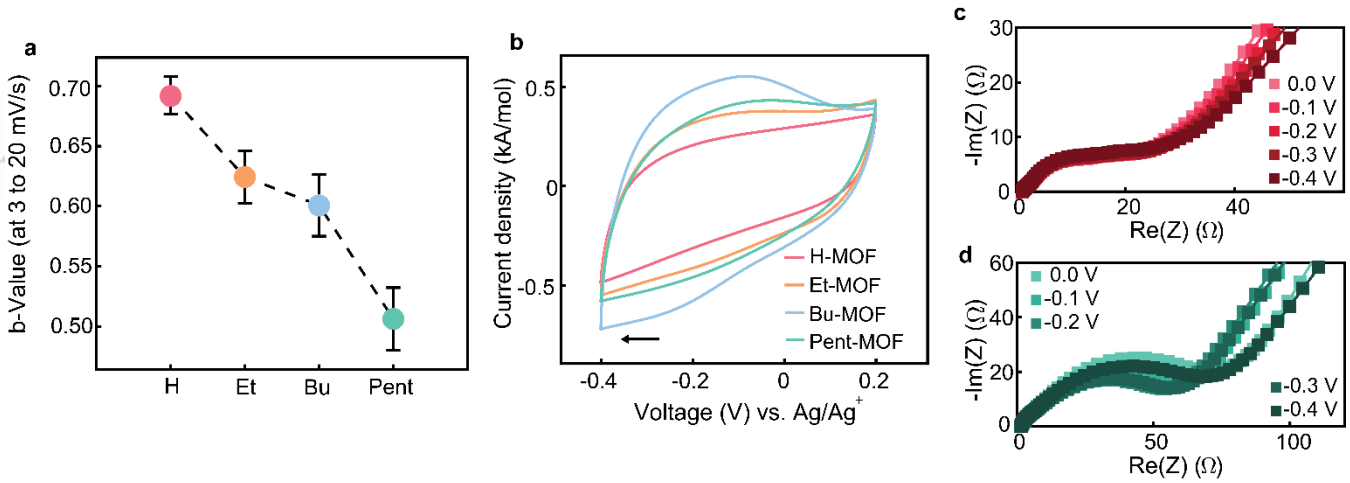

Figure 3. a) CV traces of sweeps from 0.2 to –0.4 V at a scan rate of 5 mV/s. b) b-values according to $i = av^b$, fitted to CV data collected at scan rates between 3 and 20 mV/s. Nyquist plots of c) H-MOF and d) Pent-MOF in three-electrode cell setups at various applied potentials

10.1002/anie.202402526

The increasing specific capacitances may be assigned to better access to the π-orbitals of the redox active ligands with increasing interlayer spacing. An alternative explanation for the increasing capacitance in this MOF series is, however, a potential confinement effect, whereby Li^+ ions become increasingly desolvated as they insert into the alkylated MOFs.

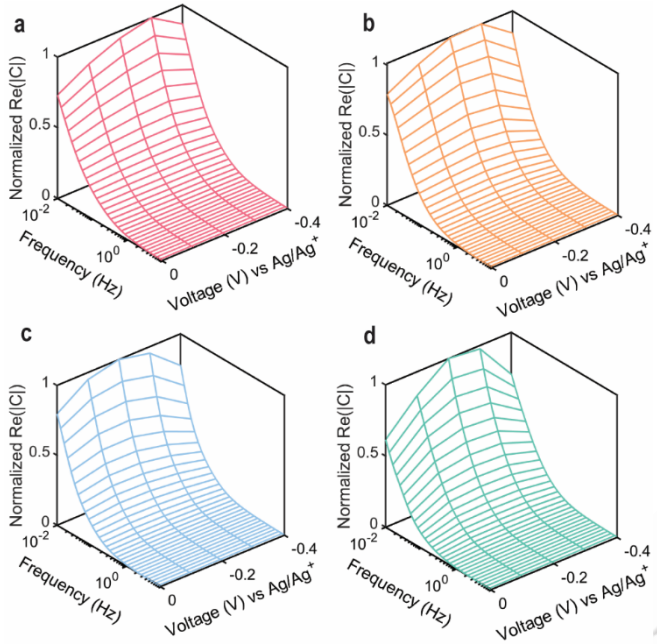

Figure 4. 3D-Bode representations of EIS of (a) H-MOF, (b) Et-MOF, (c) Bu-MOF and (d) Pent-MOF, showing the frequency and voltage dependence of the normalized real capacitance.

Analysis of the relative faradaic contributions to the overall capacitance of exfoliated MOFs allows us to distinguish between these two possibilities: Cleavage of 2D layers would lead to increased accessibility of the π-planes and can be viewed as an "infinite" increase of interlayer spacing with concomitant maximization of the electrochemically active surface area. At the same time, exfoliation would not change the pore diameter or chemical environment. Confinement is discouraged as ions would be able to access increased surface without shedding their solvation sphere.

To test the effect of exfoliation, Bu-MOF and Pent-MOF were subjected to sonochemical treatment in ethanol. After 5 h of sonication, a subtle colour change of the supernatant solution from grey-blue to a clear blue solution was observed. Centrifugation was performed to remove larger particles, and a blue colloidal solution of exfoliated MOF was obtained. Remarkably, this solution is stable under ambient conditions for at least several weeks without aggregation. The progress of exfoliation was followed via ultraviolet-visible (UV-Vis) spectroscopy. The UV-Vis spectra of the exfoliated Bu-MOF and Pent-MOF in ethanol matched their diffuse reflectance spectra as solids (**Figure S11**). Colloidal suspensions of insufficiently sonicated MOF show shifted absorbances, likely due to strong contributions of scattering on larger particles. Retention of crystal lattice of Bu-MOF was confirmed by transmission electron microscopy (TEM), clearly showing the lattice fringes of hexagonal particles (**Figure S12**). Raman spectroscopy shows bands typical for 2D materials and reveals a sharpening of bands upon exfoliation, consistent with a decrease in inhomogeneity of environments (**Figure S13**).[22]

Bode projection of the impedance spectra of the exfoliated Bu-MOF with the same electrode composition as the bulk material projection shows higher voltage dependence of the real capacitance across a wider frequency range (**Figure 5**). This clearly demonstrates the increase in faradaic contributions upon exfoliation. [19,23] The data for the exfoliated Pent-MOF mimics that of Bu-MOF (**Figure S14**). As confinement decreases while faradaic contributions increase for the exfoliated MOFs, we may rule out confinement as the major contributor to the observed increase in capacitance and faradic processes across the series of MOFs. Instead, we assign the increasing faradaic nature of charge storage to better access to the π-orbitals of the redox active ligands, caused by increasing interlayer spacing. The interactions of ions with the MOF interlayer may be viewed as the equivalent to the intercalation pseudocapacitive mechanism in non-porous structures in which lithium ions interact with active sites that reside between 2D layers.[5]

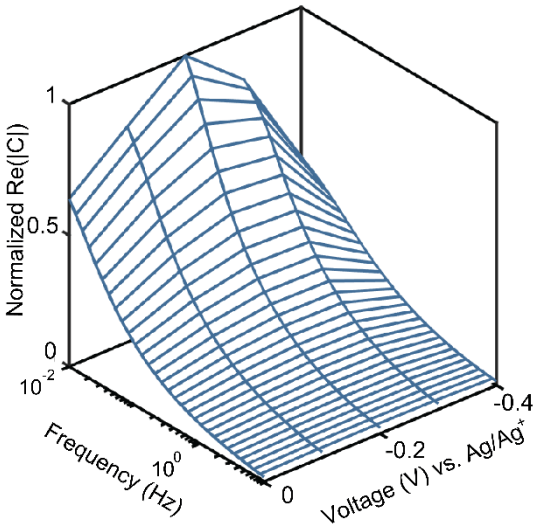

Figure 5. 3D-Bode representations of EIS of exfoliated Bu-MOF, showing the frequency and voltage dependence of the normalized real capacitance.

Through rational ligand modification of porous 2D conductive MOFs, we were able to promote faradaic processes and enhance the specific capacitance by a factor of 1.7 by increasing interlayer spacing. Electrochemical analysis allowed for deconvolution of opposite trends for resistive contributions and charge transfer-based contributions across the series of MOFs. Bulk exfoliation yielded stable colloidal solutions and further promoted faradaic processes by providing better access to redox active ligand planes. Increasing access to ligand-based active sites via interlayer distance is thus a viable strategy to introduce faradaic pseudocapacitive processes for porous 2D MOFs and bridges our understanding of porous double layer capacitors and layered intercalation-based pseudocapacitors. Our findings inspire the possibility of reaching higher energy densities compared to non-porous layered intercalation pseudocapacitors by utilizing active sites across the entire bulk. These findings might guide future material design and engineering towards electrode materials with enhanced energy and power density.

Supporting Information

The authors have cited an additional reference within the Supporting Information.[24]

Acknowledgements

AS, JW and MD acknowledge the Department of Energy (DE-SC0023288) for financial support. AV and AP acknowledge the European Research Council for financial support under the European Union's Horizon 2020 research and innovation program (grant agreement no. 770870,MOOiRE). Part of this work (SEM, TEM, Raman) made use of the MRL Shared Experimental Facilities at MIT. We would like to thank Dr. Tianyang Chen, Andrei Iliescu, Dr. Stavroula Kampouri and Julius Oppenheim for proofreading and suggestions for the manuscript.

Keywords: electrochemical capacitors • pseudocapacitance • coordination polymers

References

[1] P. Simon, Y. Gogotsi, *Nat. Mater.* **2008**, *7*, 845–853.
[2] R. Kötz, M. Carlen, *Electrochim. Acta* **2000**, *45*, 2483–2498.
[3] C. Choi, D. S. Ashby, D. M. Butts, R. H. DeBlock, Q. Wei, J. Lau, B. Dunn, *Nat. Rev. Mater.* **2020**, *5*, 5–19.
[4] H. Banda, J. H. Dou, T. Chen, Y. Zhang, M. Dincă, *Angew. Chem. Intl. Ed* **2021**, *60*, 27119–27125.
[5] H. Banda, J. H. Dou, T. Chen, N. J. Libretto, M. Chaudhary, G. M. Bernard, J. T. Miller, V. K. Michaelis, M. Dincă, *J. Am. Chem. Soc.* **2021**, *143*, 2285–2292.
[6] D. Sheberla, J. C. Bachman, J. S. Elias, C. J. Sun, Y. Shao-Horn, M. Dincă, *Nat. Mater.* **2017**, *16*, 220–224.
[7] P. Zhang, M. Wang, Y. Liu, Y. Fu, M. Gao, G. Wang, F. Wang, Z. Wang, G. Chen, S. Yang, Y. Liu, R. Dong, M. Yu, X. Lu, X. Feng, *J. Am. Chem. Soc.* **2022**, *145*, 6247–6256.
[8] M. Yu, R. Dong, X. Feng, *J. Am. Chem. Soc.* **2020**, *142*, 12903–12915.
[9] C. Nathan Hong, A. Crom, J. I. Feldblyum, M. RLukatskaya, *Chem* **2023**, *9*, 798–822.
[10] Y. Zhang, S. N. Riduan, J. Wang, *Chem. Eur. J.* **2017**, *23*, 16419–16431.
[11] S. Fleischmann, Y. Zhang, X. Wang, P. T. Cummings, J. Wu, P. Simon, Y. Gogotsi, V. Presser, V. Augustyn, *Nat. Energy* **2022**, *7*, 222–228.
[12] S.-J. Shin, J. W. Gittins, M. J. Golomb, A. C. Forse, A. Walsh, *J. Am. Chem. Soc.* **2023**, *145*, 14529–14538.
[13] S. Bi, H. Banda, M. Chen, L. Niu, M. Chen, T. Wu, J. Wang, R. Wang, J. Feng, T. Chen, M. Dincă, A. A. Kornyshev, G. Feng, *Nat. Mater.* **2020**, *19*, 552–558.
[14] Y. Lu, Z. Hu, P. Petkov, S. Fu, H. Qi, C. Huang, Y. Liu, X. Huang, M. Wang, P. Zhang, U. Kaiser, M. Bonn, H. I. Wang, P. Samorì, E. Coronado, R. Dong, X. Feng *J. Am. Chem. Soc.* **2024**, 146, 4, 2574–2582.
[15] P. Apostol, S. M. Gali, A. Su, D. Tie, Y. Zhang, S. Pal, X. Lin, V. R. Bakuru, D. Rambabu, D. Beljonne, M. Dincă, A. Vlad, *J. Am. Chem. Soc.* **2023**, *145*, 24669–24677.
[16] Y. Lu, Y. Zhang, C.-Y. Yang, S. Revuelta, H. Qi, C. Huang, W. Jin, Z. Li, V. Vega-Mayoral, Y. Liu, X. Huang, D. Pohl, M. Položij, S. Zhou, E. Cánovas, T. Heine, S. Fabiano, X. Feng, R. Dong, *Nat. Comm.* **2022**, *13*, 7240.
[17] A. J. Bard, L. R. Faulkner, *Electrochemical Methods: Fundamental and Applications*, John Wiley & Sons, Hoboken, NJ, **2001**.
[18] T. S. Mathis, N. Kurra, X. Wang, D. Pinto, P. Simon, Y. Gogotsi, *Adv. Energy Mater.* **2019**, *9*, 1902007.
[19] J. S. Ko, C. H. Lai, J. W. Long, D. R. Rolison, B. Dunn, J. Nelson Weker, *ACS Appl. Mater. Interfaces* **2020**, *12*, 14071–14078.
[20] C. Prehal, C. Koczwara, N. Jäckel, A. Schreiber, M. Burian, H. Amenitsch, M. A. Hartmann, V. Presser, O. Paris, *Nat. Energy* **2017**, *2*.
[21] C. Merlet, C. Péan, B. Rotenberg, P. A. Madden, B. Daffos, P. L. Taberna, P. Simon, M. Salanne, *Nat. Comm.* **2013**, *4*, 2701.
[22] A. C. Ferrari, J. C. Meyer, V. Scardaci, C. Casiraghi, M. Lazzeri, F. Mauri, S. Piscanec, D. Jiang, K. S. Novoselov, S. Roth, A. K. Geim, *Phys. Rev. Lett.* **2006**, *97*, 187401.
[23] S. Wang, Q. Wang, P. Shao, Y. Han, X. Gao, L. Ma, S. Yuan, X. Ma, J. Zhou, X. Feng, B. Wang, *J. Am. Chem. Soc.* **2017**, *139*, 4258–4261.
[24] Robertson, N., Parsons, S., MacLean, E. J., Coxall, R. A., & Mount, A. R. *J. Mater. Chem.* **2000**, *10*(9), 2043-2047.

10.1002/anie.202402526

WILEY VCH

COMMUNICATION

Entry for the Table of Contents

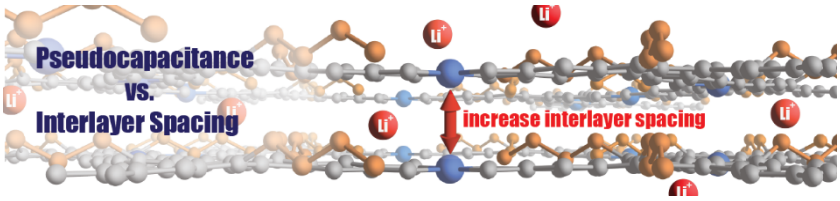

Faradaic contributions to charge storage increase as interlayer spacing widens in a series of $Ni_3(HIR_3\text{-}TAT)_2$ (R = H, Et, *n*-Bu, *n*-Pent) 2D conductive MOFs, as the charge storage mechanism shifts to adopt increasingly pseudocapacitive character. An optimum in terms of capacitance is reached, balancing faradaic contributions and resistances.